Experimental analysis of sheet metal micro-bending using a nanosecond-pulsed laser

Article *in* International Journal of Advanced Manufacturing Technology · October 2013

DOI: 10.1007/s00170-013-5032-8

4 authors, including:

Ninggang Shen
University of Iowa
47 PUBLICATIONS **334** CITATIONS
SEE PROFILE

Hongtao Ding
University of Iowa
64 PUBLICATIONS **636** CITATIONS
SEE PROFILE

Int J Adv Manuf Technol (2013) 69:319–327
DOI 10.1007/s00170-013-5032-8

ORIGINAL ARTICLE

Experimental analysis of sheet metal micro-bending using a nanosecond-pulsed laser

Chelsey Pence · Hua Ding · Ninggang Shen · Hongtao Ding

Received: 13 February 2013 / Accepted: 26 April 2013 / Published online: 10 May 2013

Abstract Laser shock bending is a sheet metal micro-forming process using shock waves induced by a nanosecond-pulsed laser. It is developed to accurately bend, shape, precision align, or repair micro-components with bending angles less than 10°. Negative bending angle (away from laser beam) can be achieved with the high-energy pulsed laser, despite the conventional positive laser bending mechanism. In this research, various experimental and numerical studies on aluminum sheets are conducted to investigate the different deformation mechanism, positive or negative. The experiments are conducted with the sheet thickness varying from 0.25 to 1.75 mm and laser pulse energy of 0.2 to 0.5 J. A critical thickness threshold of 0.7-0.88 mm is found that the transition of positive–negative bending mechanism occurs. A statistic regression analysis is developed to determine the bending angle as a function of laser process parameters for positive bending cases.

Keywords Nanosecond-pulsed laser · Laser micro-bending · Sheet metal · Negative bending

1 Introduction

Laser bending is a non-contact forming method for sheet metals, in which the sheet metal can be bent, shaped, and precision-aligned with the use of straight or curved laser scan lines to acquire desirable three-dimensional (3D) features. These features would be difficult or even impossible to manufacture using conventional metal forming techniques [1, 2]. Laser bending is of significant value to aerospace, automotive, ship building, and microelectronics industries that previously relied on expensive stamping dies and presses for prototype evaluations. Conventionally, the laser bending process is achieved by introducing thermal stress into the workpiece by irradiation with a focused laser beam. Considering both the specimen geometries and laser process conditions, material bending mechanisms by laser thermal forming technologies can be further classified into three categories: temperature gradient mechanism, buckling mechanism, and upsetting mechanism [3]. The ambient colder material caused the partial restraint of the thermal expansion in the heated area leading to deformations in the thermal forming process. With the effect of thermal expansion and shrinkage, stresses in the component are induced, which balance themselves by distortions and stress redistributions [4].

Recently, non-thermal forming using a high-energy pulsed laser has generated growing interest. Similar to the mechanical shot peening process, high-pressure and compressive shock waves are induced onto the target material by high-energy laser pulses. This non-thermal, shockwave-forming mechanism is often denoted as laser shock forming. During the process, short laser pulse irradiation duration is required, which is in the range of nanoseconds and several-orders less than the radiation time of the thermal forming mechanism. The energy of each pulse is in the range of several joules, released in nanoseconds, results in a high laser power intensity of above 1 GW/cm^2. When the high-intensity, short laser pulse is focused on the surface of the sheet metal, the surface of the sheet is vaporized and ionized immediately [5]. High-pressure plasma is then generated and expanded rapidly. With further enhancement of the confined medium layer (usually water or glass), the plasma then expands and explodes violently against the surfaces of the sheet metal. The confined layer traps the expanding vapor and plasma, and consequently causes a higher pressure shock impact in the level of over 1 GPa [6,

C. Pence · N. Shen · H. Ding (✉)
Department of Mechanical & Industrial Engineering,
University of Iowa, Iowa City, IA 52242, USA
e-mail: hongtao-ding@uiowa.edu

H. Ding
School of Automotive & Traffic Engineering, Jiangsu University,
Zhenjiang 212013, China

7]. When the peak pressure of the shock wave induced by the laser at the surface of the sheet is greater than the dynamic yield strength of the material, the sheet metal will plastically deform [8, 9]. There will be residual stress on the yield region and the sheet metal should be deformed to balance the stress.

To implement the laser bending technique in industry, it is crucial to be able to model and accurately control the bending angle of the sheet metal during the laser bending process. All of the laser parameters, scanning scheme, and work materials play critical roles in determining the bending angle. Several studies have been conducted to experimentally or numerically analyze, and quantitatively predict the bending angle during the laser sheet metal bending process. Safdar et al. [10] presented a numerical investigation of the effects of scanning schemes on bending angle, distortions, and stress distribution in laser tube bending. Their study showed that scanning schemes significantly influence laser tube bending. For the given process parameters, axial scan scheme produces twice as much bending angle as that obtained by circumferential scanning schemes. Shidid et al. [11] studied the effects of inert gas shielding on laser bending of titanium sheets with a 550 W multimode Nd:YAG laser system. Different gas flow conditions, nozzle positions, and inert gas combinations were used to enhance the bending quality and bending angle. Wielage and Vollertsen [12] investigated the dependence between deformation velocity of laser shock forming and length of the bent sample using a pulsed TEA-CO_2-laser with a wavelength of 10.6 μm, pulse duration of 100 ns, and laser shock wave pressure up to 5.6 MPa per pulse. Shen et al. [4] conducted numerical and experimental investigations to understand the edge effects in the straight line laser bending process of low carbon steel using a CO_2 laser with a 3 kW power rating. Their study showed that scanning schemes significantly influence the bending angle distribution along the scan line, and the combination of acceleration and deceleration scanning schemes can minimize the edge effects. Empirical formulas of laser bending angle have been derived to establish the relationship between the laser bending angle and process conditions. Maji et al. [13] performed experimental investigations on pulsed laser bending of AISI 304 stainless steel sheets using a 2-kW fiber laser and conducted a statistical analysis to study the effects of process parameters of laser power, scan speed, spot diameter and pulsed duration on bending angle. Gollo et al. [14] conducted laser bending experiments of 1-mm-thick mild steel AISI 1010 using a pulsed Nd:YAG laser with maximum mean laser power of 400 W. Their regression analysis showed the influence process parameters have on the bending angles. These process parameters include: material, laser power, beam diameter, scan velocity, sheet thickness, pass number, and pulse duration.

Meanwhile the laser micro-bending process has been applied to accurately control the adjustment of micro-components. Geiger and Meyer-Pittroff [15] presented contactless laser forming may serve as a solution for high precision manipulation of functional electronic or optical devices or for tuning forces as in relays-springs. Dearden and Edwardson [16] pointed out microscale applications already include the precision alignment of components during product assembly. Zhang and Xu [17] adjusted curvatures of silicon micro-cantilevers using a pulsed frequency doubled Nd:YLF laser with a wavelength of 524 nm, pulse width of 20 ns, and pulse energies of 0.18 to 0.32 μJ. Zhang and Xu [18] analyzed bending of a hard disk suspension using a laser by 3D finite element method, studied high precision microscale laser bending technique.

Up to now, most laser forming practice and research is generally focused on producing a positive bending angle, i.e., bending occurs towards the laser beam, using the laser thermal forming technologies. Comparatively, little research has been investigated on negative (away from the laser beam) bending process via high-energy nanosecond pulse laser. Liu et al. [1] and Guan et al. [2] conducted laser bending experiments on the stainless foil, producing negative bending angles using American Synrad 48-5 series CO_2 laser with a wave length of 10.6 μm and 50 W power. Their experimental results showed that negative bending angles could be produced if elastic pre-bending were induced in a direction away from the laser beam. The aforementioned research works present various instructive statements about the process parameter optimization and pretreatment of the specimen. However, during the laser micro-bending process, it would be extremely difficult to frequently deposit absorptive coatings and accurately control the laser bending. In addition, it could be an issue to remove the absorptive coating, and it was seldom reported about how to control the bending angle accurately and simply.

In this paper, in order to address the deformation control technique in laser micro-bending, various experiments for thin aluminum sheet in one-side shock configuration are conducted with a nanosecond Nd:YAG pulse laser device. The bending angle evaluated in this research is less than 10°, which is usually the deformation problem of sheet metal generated in assembly processes. The effects of laser pulse energy, scanning scheme, and sheet thickness are examined. The positive or negative bending mechanisms are numerically analyzed with a finite element (FE) model developed in ABAQUS.

2 Evaluation of the nanosecond-laser-induced pressure

A schematic of the nanosecond-laser-induced shock wave is depicted in Fig. 1, in which a powerful pulse laser beam with laser power intensities above 1 GW/cm^2 is focused to peen the target metal surface. A translucent layer consisting of flowing water is employed over the specimen and acts as

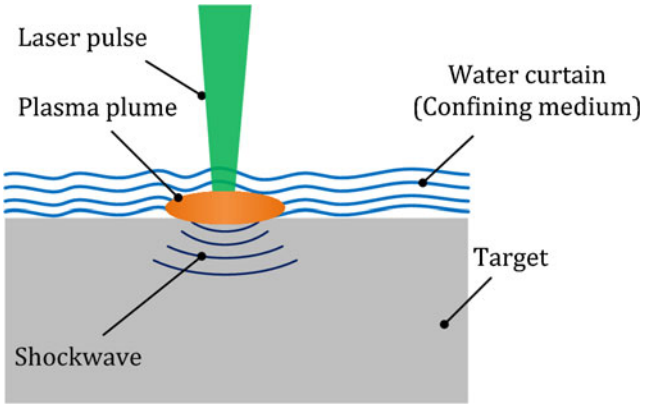

Fig. 1 Generation of laser-induced shock wave

a confined medium directing the shock wave into the treated material. Short laser pulses with a time period of about 6–8 ns are focused to explode the ablative coating, resulting in a high-pressure shock wave with a peak pressure of 2–10 GPa [5, 6]. The laser-induced shock wave then propagates into the substrate material to generate plastic deformation with a compressive layer as deep as about 1 mm [19]. A larger area of interest can be processed by a multi-track laser scan, which is achieved by repositioning the laser beam with high precision motorized stages and computer-control. The surface is pressed and elongated to the lateral direction plastically, and the sheet metal is bent. Laser shock forming is achieved by scanning the laser over whole or local area of the surface and accumulating such deformations.

It is critical to determine and control the laser-induced shock pressure for the bending process. Many attempts have been carried out in recent years to model and predict the shock wave pressure induced by the laser-matter interaction. Fabbro et al. [20] proposed a simple analytical model using two free variables, which has been widely used in numerical analyses on different aspects of laser shock peening processes such as predictions of indentation profile and residual stresses [21–25]. Wu and Shin [26] have developed a self-closed thermal model for the confined plasma in the LSP process without using any free variables, but considering most of the important relevant physical processes. By applying the confined plasma model to the FE analysis of LSP, Cao et al. [19] accurately modeled the indentation profile and residual stresses of various metallic specimens, such as 4140 steel, 316L stainless steel, and Ti6Al4V alloy under different LSP conditions. Recently, Wu and Shin [5] have developed a numerical model with stricter physics consideration, where the one-dimensional hydrodynamic equations governing the conservation of mass, momentum, and energy for the confining medium and metal targets are supplemented with appropriate equations of state. For nanosecond-laser pulses with irradiances of several GW/cm^2, the plasma induced by laser ablation of metal targets could be described by the hydrodynamic equations for the whole physical domain, where the condensed phase contributes mass to the plasma region mainly through hydrodynamic expansion. Therefore, this hydrodynamics model is adopted in this study to calculate the laser-induced shock pressure.

According to the criteria developed by Wu and Shin [27], 1D plasma expansion assumption is valid when the laser beam diameter is equal or larger than 300 μm. Since the laser beam diameter used in this work is around 3 mm, it is sufficient to use the 1D model in this work to describe the confined plasma behavior under air or water. For this system, the 1D hydrodynamic equations governing conservation of mass, momentum, and energy, can be expressed as

$$\frac{\partial}{\partial t}\begin{bmatrix}\rho_1\\ \rho_2\\ \rho u\\ E_i+\frac{1}{2}\rho u^2\end{bmatrix}+\frac{\partial}{\partial y}\begin{bmatrix}\rho_1 u\\ \rho_2 u\\ \rho u^2+P\\ u\left(E_i+\frac{1}{2}\rho u^2+P\right)\end{bmatrix}=\frac{\partial}{\partial y}\begin{bmatrix}0\\ 0\\ 0\\ -q+k\frac{\partial T}{\partial y}+I\end{bmatrix} \tag{1}$$

where ρ_1 and ρ_2 are the densities of metal and air (or water), respectively. ρ is the total density defined as $\rho=\rho_1+\rho_2$, u is the velocity, P the pressure, E_i the volumetric internal energy, T the temperature, k the thermal conductivity, I the net flux in laser radiation, and q the radiative heat flux out of the domain. To obtain the radiative heat flux, the radiative transfer equation needs to be solved in the diffusion approximation:

$$q=\int_v q_v dv, \qquad \frac{\partial q_v}{\partial y}+ck_vU_v=ck_vU_{bv}$$
$$q_v=-\frac{c}{3k_v}\frac{\partial U_v}{\partial y}, \qquad U_{bv}=\frac{8\pi hv^3}{c^3\left(e^{hv/kT}-1\right)} \tag{2}$$

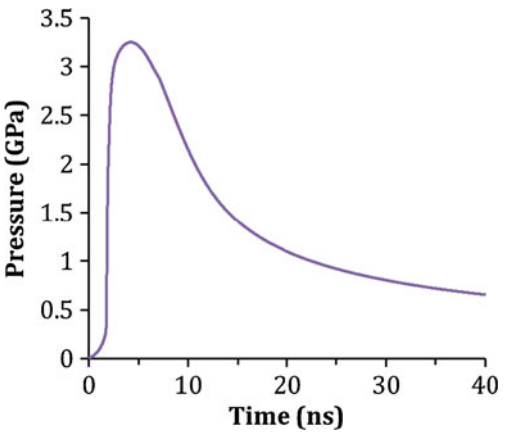

Fig. 2 Laser-induced shockwave pressure

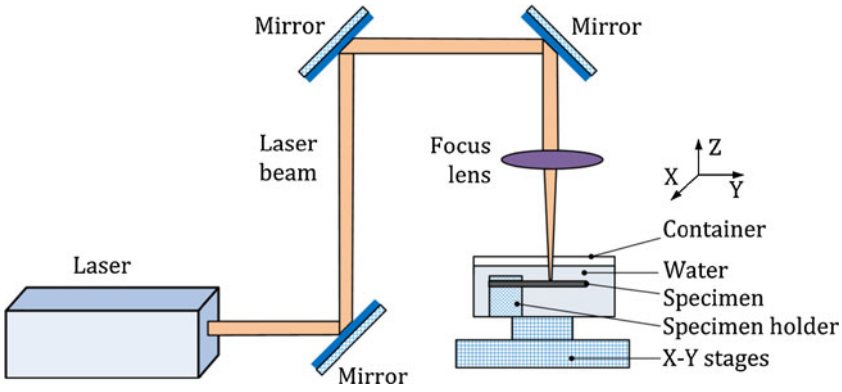

Fig. 3 Experiment setup

in which c is the speed of light, U_v and U_{bv} are the spectral energy density of plasma radiation and blackbody radiation, respectively. k_v is the absorption coefficient, and index 'v' denotes frequency dependent quantities. To solve the hydrodynamic equations, wide-range equations of state (EOS) have been supplemented. For the metal targets, the quotidian equation of state (QEOS) is applied, which is an equation of state model for hydrodynamic simulation of high-pressure phenomena. Many complicated phenomena are considered, such as the ionization process and the chemical equilibrium among dissociation products of water. Figure 2 shows the laser-induced shock pressure durations in water medium for aluminum target material calculated using the hydrodynamics model using the laser processing conditions. It is noted that the normalized pressure profiles for different laser power densities are very similar: the pressure increases drastically during the laser pulse duration, and then gradually drops to below 15 % of the peak value.

3 Experiments

The laser shock bending process equipment used in this study is shown in Fig. 3. A Q-switched Nd:YAG laser with a wavelength of 1064 nm was used in the experiment, with a laser pulse repetition rate of 10 Hz and pulse duration of 7 ns. The laser pulse energy, E, was adjustable. The laser beam was conducted to the target through a series of reflecting mirrors and a convergent lens with a focal length of 35 mm to a laser spot size, d, of 1.75 mm on the surface of specimen, as shown in Fig. 3. The specimen was fixed at one end on a worktable in a water tank, which produced a water-confinement regime. The depth of water-confinement layer was set to 10 mm from the specimen. The movement of specimen in X and Y direction was controlled by two linear motion stages with a motion resolution of 0.01 mm.

The Aluminum 1060 sheet metals were used as the specimens in this research. Each specimen was cut to 76 mm×

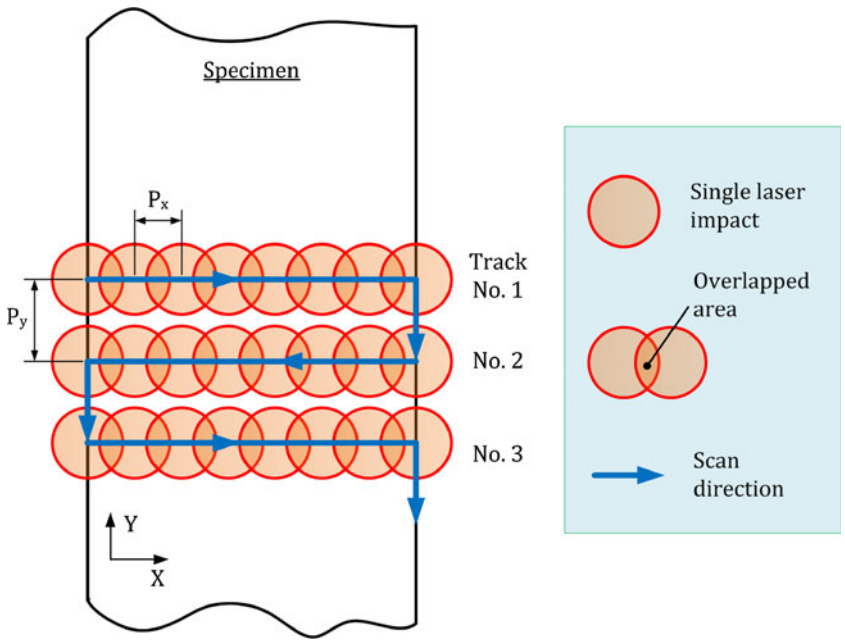

Fig. 4 Laser scanning path

Table 1 Experimental conditions

Parameters	Parameter range
Pulse energy, E (J)	0.2, 0.25, 0.3, 0.4, 0.5
Specimen thickness, t (mm)	0.25, 0.70, 0.88, 1.07, 1.75
No. tracks, n	1, 2, 3, 5
Scanning speed, V (mm/s)	5, 7.5, 10
Overlapping ratio, OR	44 %, 53 %, 63 %

19 mm in size and had an initial bending angle less than 15'. Before laser impact, the specimens were cleaned with acetone. In order to create a bulk, uniform bending of the large specimen, the laser scanned over the targeted surface area of the clamped specimen by moving the X–Y stage. The laser scan path is shown in Fig. 4. The laser starts from one free side of the specimen, moves linearly across the specimen surface, moves over to the next position, and then reverses the track. Constant laser scan speed, V, was used in one test, which produced a constant distance, P_x, between the two adjacent laser impacts as well as the overlapping area of the two laser pulses. The distance between the two laser scan lines, P_y, was kept as 2 mm. The experimental conditions are given in Table 1. The specimen thickness varied from 0.25 to 1.75 mm, laser pulse energy varied from 0.2 to 0.5 J, laser scan speed varied from 5 to 10 mm/s, and the number of laser scan tracks varied from 1 to 5 per test. The overlapping ratio of the adjacent laser impacts was dependent on the laser scan speed, and varied from 44 to 63 %.

The sketch of the specimen constraint and bending angle measurement after the experiment are shown in Fig. 5. The profile of the bending angle was captured by a tool microscope (JGX-type 1), and the edge lines of the image were detected by image process software, then the bending angle could be obtained by calculating the difference in the slopes of the two edge lines. The measurement had an accuracy of 1' per measurement. As can be seen in Fig. 5, a positive bending angle is defined as bending towards the laser beam, while a negative bending angle is defined for bending away from the laser beam. It should be noted that the bending angle evaluated

Table 2 Experimental results

Test	t (mm)	I (GW/cm^2)	E (J)	OR (%)	V (mm/s)	n	θ (')
1	0.70	1.2	0.20	63	5	5	65
2	0.88	1.2	0.20	63	5	5	−2
3	1.07	1.2	0.20	63	5	5	−9
4	1.75	1.2	0.20	63	5	5	−28
5	0.70	1.8	0.30	63	5	5	127
6	0.88	1.8	0.30	63	5	5	−1
7	1.07	1.8	0.30	63	5	5	−9
8	1.75	1.8	0.30	63	5	5	−28
9	0.70	2.4	0.40	63	5	5	130
10	0.88	2.4	0.40	63	5	5	22
11	1.07	2.4	0.40	63	5	5	−13
12	1.75	2.4	0.40	63	5	5	−29
13	0.70	3.0	0.50	63	5	5	133
14	0.88	3.0	0.50	63	5	5	27
15	1.07	3.0	0.50	63	5	5	−16
16	1.75	3.0	0.50	63	5	5	−31
17	0.25	1.2	0.20	44	10	1	18
18	0.25	1.2	0.20	53	7.5	2	118
19	0.25	1.2	0.20	63	5	3	176
20	0.25	1.5	0.25	44	10	2	146
21	0.25	1.5	0.25	53	7.5	3	396
22	0.25	1.5	0.25	63	5	1	132
23	0.25	1.8	0.30	44	10	3	310
24	0.25	1.8	0.30	53	7.5	1	102
25	0.25	1.8	0.30	63	5	2	376

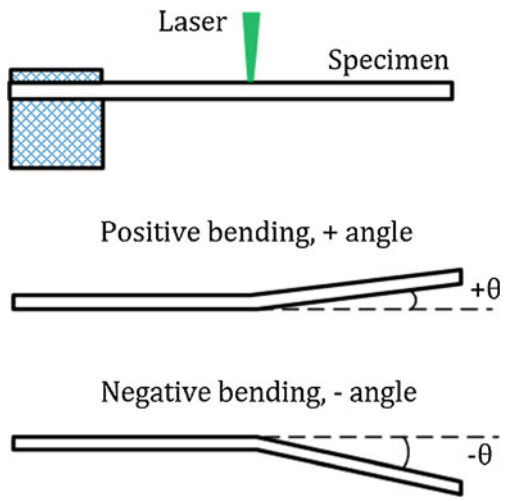

Fig. 5 Bending angle measurement

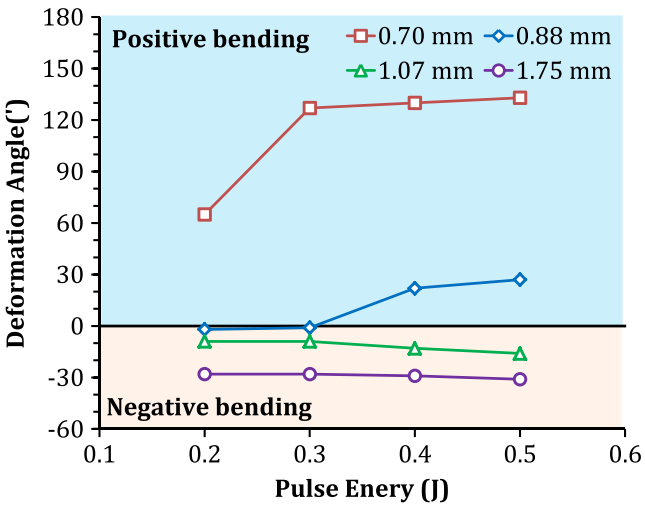

Fig. 6 Bending angles for various laser pulse energies

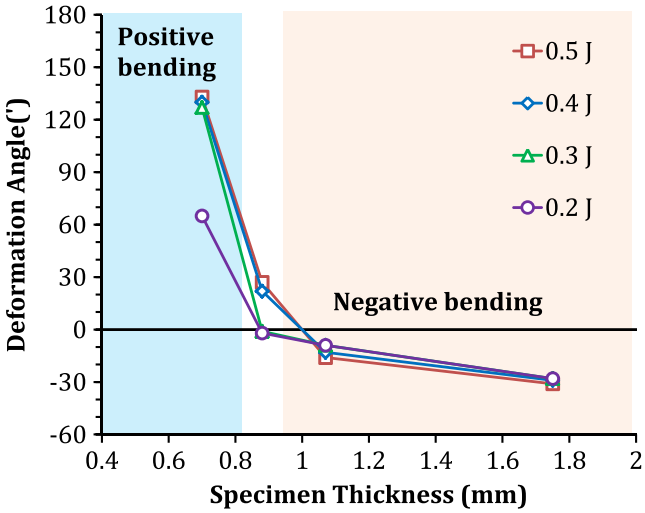

Fig. 7 Bending angles for various sheet metal thicknesses

in this research is less than 10°, which is usually the deformation problem of sheet metal generated in assembly process.

4 Results and discussions

The laser shock micro-bending experimental results are shown in Table 2. In Tests 1–16, the positive–negative bending mechanisms were investigated extensively for a full factorial design of various specimen thicknesses and laser pulse energies. Four different specimen thicknesses, 0.7, 0.88, 1.07, and 1.75 mm, and four different laser pulse energies, 0.2, 0.3, 0.4, and 0.5 J (power density ranging from 1.2 to 3 GW/cm^2), were tested. Other process parameters such as laser spot size, overlapping ratio (or laser scan speed) and number of scan tracks were set constant. Note both positive and negative bending angles were obtained from these tests. To ensure the repeatability of the experimental data, multiple laser shock bending tests were conducted for each test condition.

Tests 17–25 were performed on specimens of 0.25 mm thickness in the domain of positive bending. The effect of process parameters such as laser pulse energy, laser scan speed and number of scan tracks were studied. A three-level and three-factor design of experiments was implemented for nine conditions as shown in Table 2. The laser pulse energy ranged from 0.2 to 0.3 J (or pulse power density of 1.2–1.8 GW/cm^2), overlapping ratio ranged from 44 to 63 % (or laser scan speed of 5–10 mm/s), and number of scan tracks ranged from 1 to 3. More scan tracks produced a bending angle of more than 10° for the 0.25-mm-thick specimens, which were not discussed in this study.

4.1 Negative bending mechanism

Figure 6 shows the bending angles with different laser pulse energies for different specimen thicknesses. Positive bending was clearly observed in the specimen of 0.7 mm thickness, while negative bending appeared dominate for thicker specimens with thickness of 1.07 and 1.75 mm. No apparent bending was observed for specimen of 0.88 mm thickness when the laser pulse energy was low (0.2–0.3 J); however, as the laser pulse energy increased to 0.4–0.5 J positive bending angle of about 27′ was measured. The laser energy input in the case of thinner specimens (<0.88 mm) drives more deformation and hence larger positive bending angle. For instance, as the laser pulse energy increased from 0.2 to 0.5 J, the sheet bending angle increased from 65′ to 133′ for the specimens of 0.7 mm thickness. No significant effect can be found for laser pulse energy on negative bending angle. It appeared that the negative bending angle saturated at around −15′ and −30′ for 1.07- and 1.75-mm thick specimens, respectively.

The effect of specimen thickness was closely examined in Fig. 7. The specimen thickness is apparently the dominant factor in positive–negative bending transition. The bending angle changes from positive to negative as the specimen thickness increases. When the specimens were thin (0.7 mm), positive bending angle was obtained for the laser pulse energy ranging from 0.2 to 0.5 J. When the specimen thickness increased to above 1.07 mm, negative bending angle was obtained for all the laser pulse energies tested. A specimen with thickness of 0.88 mm appeared to locate in the transition area from positive to negative.

During the laser shock bending process, plastic deformation occurs to a depth where the laser-induced shock wave

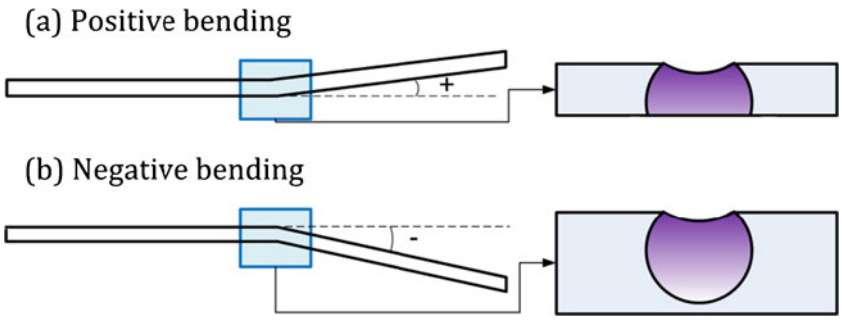

Fig. 8 Laser shock forming mechanisms

Table 3 Mechanical properties of Aluminum 1060

Property	Value
Density (kg/m^3)	2,672
Poisson's ratio, ν	0.33
Elastic modulus (GPa)	72.4
Hugoniot elastic limit, HEL (GPa)	0.6

pressure no longer exceeds the metal's Hugoniot elastic limit (HEL). The HEL of the target metal is related to the dynamic yield strength by [28]:

$$\mathrm{HEL} = \frac{1-\nu}{1-2\nu}\sigma_{\mathrm{y}}^{\mathrm{dyn}} \tag{3}$$

where ν is Poisson's ratio and σ_y^{dyn} is the dynamic yield strength at high strain rates. The HEL of the work material Aluminum 1060 was evaluated to be 0.6 GPa [29]. When the laser-induced shock wave peak pressure is less than the material HEL, no plastic deformation occurs and no residual stress is induced either. As the shock wave pressure is above 1 HEL, plastic deformation and plastic strain increase further and reach deeper into the target material. Therefore, the ratio of depth of laser pulse-induced plastic deformation and the specimen thickness, λ, is determined by the laser-induced shock wave pressure, shock wave duration, work material properties and work material thickness, etc. Under the same laser parameters, the increase of specimen thickness decreases the ratio λ, and vice versa. The laser positive-to-negative bending mechanism can be illustrated using the ratio λ as shown in Fig. 8. As the ratio λ equals unity, i.e., the specimen is thoroughly strained, positive bending angle forms. As the ratio λ is significantly less than unity, negative bending takes place.

To numerically delineate the positive-to-negative bending mechanism, the laser shock micro-bending tests of 13 and 16 of two specimen thicknesses were simulated using a finite element model adopted from [6] with the commercial software ABAQUS 6.12-1. The workpiece domain is meshed using four-node thermally coupled axisymmetric quadrilateral, bilinear displacement, and temperature elements using reduced integration and enhanced hourglass control. Mechanical properties of Aluminum 1060 are shown in Table 3. The laser-induced shock wave pressures predicted using the hydrodynamics model were applied as user-defined distributed time-dependent pressure loads in ABAQUS. To capture the dynamic nature of the shock wave in each LSP impact, fully coupled thermo-mechanical ABAQUS/Explicit analysis was first carried out for a time step of 2,000 ns. The resultant solution was then imported to the following implicit step, which calculates the steady-state deformation by the ABAQUS/Standard solver to save computation cost. The simulation results of laser shock bending deformation are shown in Fig. 9. Under the same laser energy loading conditions, the ratio λ declines significantly as the specimen thickness increases from 0.7 to 1.75 mm, and the laser bending mechanism changes from positive to negative. It can be seen in Fig. 9 that the predictions of the bending angles and deformation are very close to the measurements at various specimen thicknesses.

4.2 Positive bending angle analysis

It is desirable that a relationship will be developed to determine the bending angle as a function of laser process parameters. Although bending angles appears saturated in the negative bending domain, positive bending angle is critically affected by the laser process parameters when the specimen thickness is thin. A multivariable regression analysis using the experimental data from Tests 1, 5, 9, 13, and 17–25 was conducted to establish a statistical model, which determines the sheet metal bending angle (θ, °). Four independent variables; sheet thickness (t, mm), laser pulse power intensity (I, GW/cm^2), overlapping ratio (OR), and passes of tracks (n) were selected as the four factors for this statistical analysis. The obtained equation shows the predicted correlation between laser parameters and the sheet bending angle, which works well with estimation residuals less than 15 %.

$$\theta = 13.64 I^{0.41} t^{-1.92} OR^{1.84} n^{1.16} \tag{4}$$

Note Eq. 4 only applies to positive bending for specimen thickness less than 0.7 mm. As can be seen in Eq. 4, specimen thickness plays an important role and has an adverse negative effect on the positive bending angle. The bending angle rises with the increase of overlapping ratio, passes of tracks, and laser pulse power intensity.

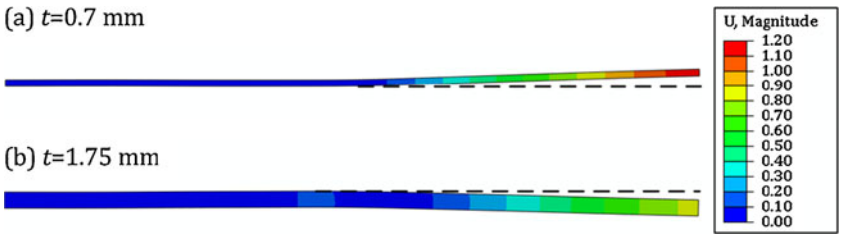

Fig. 9 Finite element simulation of laser shock bending

5 Conclusions

The deformation of the laser micro-bending was determined with the specimen thickness and laser energy. The test results show that with the same laser parameters, thickness of the specimens is the dominant factor to determine the deformation mechanism of the sheet. Comparing the thickest specimen of 1.75 mm and the thinnest specimen of 0.25 mm, it is clear that the deformation mechanism of the 0.25-mm-thick sheet will be positive under all laser energy conditions, while the deformation mechanism of the 1.75-mm-thick sheet will be negative under all laser energy conditions. When the specimen thickness gets thinner, the laser energy has more significant positive effects on the deformation of the sheet in the positive deformation mechanism conditions. The bending angle can hardly change with the increase of the laser energy in the negative deformation mechanism. It appeared that the negative bending angle can saturate at some certain value, such as around −15′ and −30′ for 1.07- and 1.75-mm-thick specimens, respectively.

A critical thickness threshold of 0.7–0.88 mm is found where the transition of positive–negative bending mechanism occurs. When thickness is greater than the threshold, the deformation mechanism is negative; when the thickness is less than the threshold, deformation mechanism is positive. A finite element simulation proved that as the specimen is thoroughly strained, positive bending angle forms; as the ratio of depth of laser pulse-induced plastic deformation and the specimen thickness significantly less than unity, negative bending takes place. Positive bending angle is critically affected by the laser process parameters when the specimen thickness is thin. An empirical correlation equation was obtained by multiple regressions based on the positive bending experiments. The bending angle rises with the increase of overlapping ratio, passes of tracks, and laser pulse power intensity, but decreases with the specimen thickness.

Acknowledgments The authors wish to gratefully acknowledge the financial support provided for this study by the National Science Foundation under Grant Number EPS-1101284.

References

1. Liu J, Sun S, Guan Y, Ji Z (2010) Experimental study on negative laser bending process of steel foils. Opt Lasers Eng 48(1):83–88
2. Guan Y, Zhang H, Liu J, Sun S (2012) Laser micro-bending process based on the characteristic of the laser polarization. J Mater Process Technol 212(3):662–671
3. Geiger M, Vollertsen F (1993) The mechanisms of laser forming. CIRP Ann Manuf Technol 42(1):301–304
4. Shen H, Hu J, Yao Z (2010) Analysis and control of edge effects in laser bending. Opt Lasers Eng 48(3):305–315
5. Wu B, Shin YC (2007) A one-dimensional hydrodynamic model for pressures induced near the coating–water interface during laser shock peening. J Appl Phys 101:023510
6. Ding H, Shin YC (2012) Dislocation density-based modeling of subsurface grain refinement with laser-induced shock compression. Comput Mater Sci 53(1):79–88
7. Wu B, Shin YC (2007) From incident laser pulse to residual stress: a complete and self-closed model for laser shock peening. J Manuf Sci Eng Trans ASME 129:117–125
8. Li J, Cheng GJ Forming limit and fracture mode of microscale laser dynamic forming. In: 4th Pacific International Conference on Applications of Lasers and Optics, PICALO 2010, March 23, 2010 - March 25, 2010, Wuhan, China, 2010. 4th Pacific International Conference on Applications of Lasers and Optics, PICALO 2010. Laser Institute of America
9. Ye C, Cheng GJ (2010) Effects of temperature on laser shock induced plastic deformation: the case of copper. J Manuf Sci Eng Trans ASME 132:0610091–0610098
10. Safdar S, Li L, Sheikh MA, Zhu L (2007) Finite element simulation of laser tube bending: effect of scanning schemes on bending angle, distortions and stress distribution. Opt Laser Technol 39(6):1101–1110
11. Shidid DP, Gollo MH, Brandt M, Mahdavian M (2013) Study of effect of process parameters on titanium sheet metal bending using Nd:YAG laser. Opt Laser Technol 47:242–247
12. Wielage H, Vollertsen F (2011) Classification of laser shock forming within the field of high speed forming processes. J Mater Process Technol 211(5):953–957
13. Maji K, Pratihar DK, Nath AK (2013) Experimental investigations and statistical analysis of pulsed laser bending of AISI 304 stainless steel sheet. Opt Laser Technol 49:18–27
14. Gollo MH, Mahdavian SM, Naeini HM (2011) Statistical analysis of parameter effects on bending angle in laser forming process by pulsed Nd:YAG laser. Opt Laser Technol 43(3):475–482
15. Geiger M, Meyer-Pittroff F (2002) Laser beam bending of metallic foils.187–190
16. Dearden G, Edwardson SP (2003) Some recent developments in two-and three-dimensional laser forming for 'macro' and 'micro' applications. J Opt A Pure Appl Opt 5(4):S8
17. Zhang X, Xu X (2005) Laser bending for high-precision curvature adjustment of microcantilevers. Appl Phys Lett 86(2):021114
18. Zhang X, Xu X (2005) Laser bending for adjusting curvatures of hard disk suspensions. Microsyst Technol 11(11):1197–1203
19. Cao Y, Shin YC, Wu B (2010) Parametric study on single shot and overlapping laser shock peening on various metals via modeling and experiments. J Manuf Sci Eng Trans ASME 132:0610101–06101010
20. Fabbro R, Fournier J, Ballard P, Devaux D, Virmont J (1990) Physical study of laser-produced plasma in confined geometry. J Appl Phys 68:775–784
21. Peyre P, Chaieb I, Braham C (2007) FEM calculation of residual stresses induced by laser shock processing in stainless steels. Model Simul Mater Sci Eng 15:205–221
22. Amarchinta HK, Grandhi RV, Clauer AH, Langer K, Stargel DS (2010) Simulation of residual stress induced by a laser peening process through inverse optimization of material models. J Mater Process Technol 210(14):1997–2006
23. Braisted W, Brockman R (1999) Finite element simulation of laser shock peening. Int J Fatigue 21(7):719–724
24. Hu Y, Yao Z, Hu J (2006) 3-D FEM simulation of laser shock processing. Surf Coat Technol 201(3–4):1426–1435
25. Achintha M, Nowell D (2011) Eigenstrain modelling of residual stresses generated by laser shock peening. J Mater Process Technol 211(6):1091–1101

26. Wu B, Shin YC (2005) A self-closed thermal model for laser shock peening under the water confinement regime configuration and comparisons to experiments. J Appl Phys 97:113517
27. Wu B, Shin YC (2007) Two dimensional hydrodynamic simulation of high pressures induced by high power nanosecond laser-matter interactions under water. J Appl Phys 101:103514
28. Montross CS, Wei T, Ye L, Clark G, Mai Y-W (2002) Laser shock processing and its effects on microstructure and properties of metal alloys: a review. Int J Fatigue 24(10):1021–1036
29. Ding H, Wang Y, Cai L (2010) Laser shock forming of aluminum sheet: finite element analysis and experimental study. Appl Surf Sci 256(6):1703–1707